www.czasopisma.pan.pl PAN POLSKA AKADEMIA NAUK www.journals.pan.pl

Arch. Metall. Mater. **66** (2021), 3, 853-860

DOI: 10.24425/amm.2021.136390

D. SOBOŃ[1*]

EFFECT OF LASER SURFACE MELTING ON MICROSTRUCTURE OF COLD SPRAYED Ni20Cr COATINGS

In this study, Ni20Cr coatings were obtained by cold spraying on an aluminum alloy 7075 substrate. The obtained coatings were characterized by a uniform microstructure and low porosity. The sprayed coating has the same phase composition as the powder used. Next, the cold sprayed coatings were heat treated using a TRUMPF TLF 6000 TURBO (4 kW) CO_2 laser. The laser surface melting of the coatings resulted in the formation of a columnar structure and an improvement in their mechanical properties. The Ni20Cr cold sprayed coatings after additional laser melting showed lower porosity and an increase in microhardness and Young`s modulus.

Keywords: cold spraying, Ni20Cr coating, laser modification, mechanical properties

1. Introduction

A new solution in the area of surface engineering is associated with the possibility of modifying already used techniques. This also applies to thermal spraying technology, which allows the application of coatings with very good properties from various materials [1-4]. Particularly interesting is cold spraying (CS), which allows coatings to be obtained with properties that are unattainable by conventional thermal spraying methods. The cold gas process involves the deposition with the high kinetic energy of powder particles which are accelerated in high-pressure process gas in a De Laval nozzle at supersonic speed (500-1200 m/s) hitting the substrate. The deposition of the coating occurs through intense deformation of powder particles, which causes them to adhere closely to each other [5-8]. During the CS process, metallic particles, hitting the substrate at high speed, activate and roughen the surface, increasing the adhesion of the coating to the substrate and deposition rate. The surface roughness of the substrate affects the coating adhesion [9-10], while the powder morphology and parameters of the spraying process influence the microstructure and mechanical properties of coatings. Additionally, coatings deposited at high temperature and pressure of working gas possess very low porosity [11,12].

The CS process is a low-temperature coating technology that occurs in a solid-state at a temperature below the melting point of the sprayed powder, which eliminates the detrimental effects associated with a change in phase composition of solid particles, particle oxidation, evaporation, gas release, shrinkage, porosity, and other defects found in traditional thermal spraying processes. The occurrence of low temperatures in the cold spraying process is desirable while striving to maintain the elemental composition of the powder used [8].

A laser beam is recommended for surface treatment, especially for laser surface melting. This is one of the most beneficial techniques because it is possible to process a specific area. Lasers transmit narrow and coherent energy in the visible light range. This technique is recommended due to the lack of the disadvantages associated with conventional methods of heat treatment and is often used to increase the adhesion and cohesion of thermally sprayed coatings, which results in a significant improvement in their properties [1,13-17]. As a result, the applicability of laser-treated coatings for commercial applications is increasing [18,19]. The High Velocity Oxygen Fuel (HVOF) and plasma sprayed Ni20Cr coatings are widely used in many branches of industry. Ni20Cr coatings obtained in the thermal spraying processes are used to improve the wear resistance of components, especially at high temperatures. These coatings are obtained by traditional thermal spraying methods (plasma and HVOF) [20-22]. The Ni20Cr coatings can be applied up to 980°C. The cold gas spraying technology allows obtaining Ni20Cr coatings with a structure different than in the case of traditional methods. In addition, during this process, no changes in phase composition take place in the sprayed powder.

There are some results in the literature regarding the properties of thermally sprayed Ni20Cr coatings [1-3], but no studies have been conducted on Ni20Cr coatings deposited by cold

[1] KIELCE UNIVERSITY OF TECHNOLOGY, 7 TYSIĄCLECIA PAŃSTWA POLSKIEGO AV., 25-314 KIELCE, POLAND

* Corresponding author: dsobon@tu.kielce.pl

spraying after laser treatment. The aim of this study is to assess the impact of laser surface melting on the properties of Ni20Cr coatings sprayed with cold gas.

2. Experimental procedures

Coatings were sprayed using the Impact Innovations 5/8 cold spray system equipped with a Fanuc M-20iA robot. The gas used in the spraying was helium. In the cold gas spraying process, Ni20Cr powder (Metco 43VF-NS) with a grain range of 5-45 µm was used. The substrate was an aluminum alloy (Al 7075) prepared by grit-blasting (air, 0.5 MPa) with corundum with grain size 600-710 µm. The surface roughness after this treatment was 6.1 µm. The coatings were sprayed according to the parameters shown in Table 1.

TABLE 1

Parameters of cold sprayed Ni20Cr coatings

Parameter	Value
Pressure, MPa	4
Temperature, °C	800
Standoff distance, mm	50
Powder feeder rate, g/min	95 ±3
Speed of robot arm, m/s	0.3

The surface of the sprayed coatings was laser melted with a TRUMPF TLF 6000 TURBO (4 kW) CO_2 laser. The laser surface melting was performed by means of a rectangular beam, the total impact image of which is 20×1 mm, using a segmented mirror. The shielding gas used in the process was argon, with a gas flow rate of 15 l/min, fed coaxially to the laser beam. The laser surface melting parameters are shown in Table 2. Scanning electron microscopy (Jeol JSM-7100 F, E-SEM FEI XL 30) was used to characterize the morphology of the powder used, metallographic examination, and the analysis of the obtained coatings. The cross-sections of the laser melted coatings were cut perpendicular to the direction of movement of the laser beam. The samples were cut using a TopTech CLD-50 cutter with a diamond disk. During the entire procedure, the cutting element was in a water bath to prevent excessive overheating. For observation, the samples were embedded in synthetic resin, then ground with sandpaper of various gradations, starting with the largest, and then polished in a diamond suspension with gradations: 3 µm, 1 µm, 0.25 µm. The laser melted surface of the coating was etched with 10% oxalic acid.

TABLE 2

Parameters of laser melting of the Ni20Cr coatings

Parameter	Value
Power, W	4000
Distance, mm	8
Spot, mm,	20 × 1
Speed, m / min,	1

The phase composition analyses of the used powders and resulting coatings were performed by X-ray diffraction (XRD) using a Bruker D8 Discover diffractometer with Co Kα filtered radiation (geometric Bragg-Brentano (θ-2θ), time/step = 1.8 s, step size = 0.02°). Hardness measurements (HV0.3) were made with a Nexus 4303 hardness tester with a Vickers indenter with an applied load of 2.94 N and an exposure time of 10 s. The hardness result in each case was the average of 5 measurements made according to ISO 6507-1: 2018 (en) [23]. The powder grain size distribution was evaluated using a Malvern Mastersizer 3000. The surface topography parameters and profile shape of the coatings were tested using a Talysurf CCI Lite optical profilometer.

3. Results and discussion

Fig. 1 shows the morphology and cross-section of the Ni20Cr powder. Chemical composition of the powder (% wt); 76.5 Ni, 19.5 Cr, 1.2 Si, 1.0 Fe, 1.5 Mn, 0.5 others [24]. The pow-

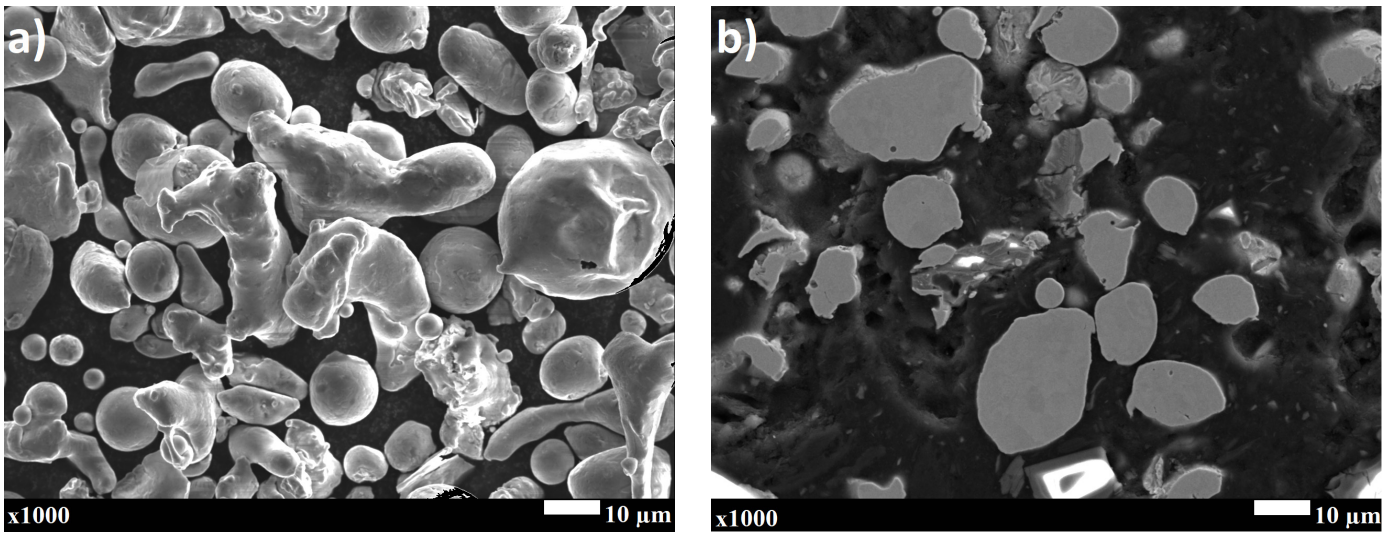

Fig. 1. a) Morphology and b) cross-sections of the Ni20Cr powder

der consist of a metallic phase. The parameters of the Ni20Cr powder (d10 = 12.92 µm, d50 = 24.99 µm, d90 = 52.73 µm) revealed that it consisted of larger grains than those declared by the manufacturer. Ni20Cr grains have a spherical or irregular shape, which is the result of water atomization, Fig. 1a. The cross-section of the powder grains shows negligible porosity and no inclusions, Fig. 1b.

The XRD analysis in Fig. 2. showed that the Ni20Cr powder consists of a Ni-Cr cubic phase with the lattice parameter (a = 3.547 Å) close to that of the Cr0.25Ni0.75 phase (a = 3.552 Å). The Cr0.25Ni0.75 phase was composed of 22.8 wt% of Cr and 77.2 wt% of Ni, according to the PDF 04-003-7001 card [25].

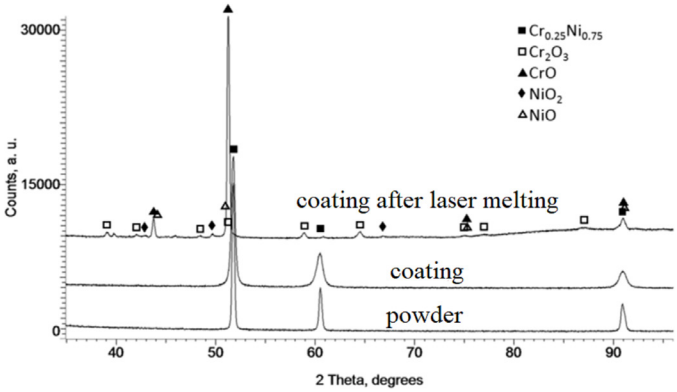

Fig. 2. XRD patterns of Ni20Cr powder and cold sprayed coating before and after laser melting

The microstructure of the cold sprayed Ni20Cr coating is shown in its cross-section, Fig. 3. The resulting coating revealed a lamellar structure characteristic of the thermal spray process. Powder particles with adequate ductility during the cold spray process hit the ground and formed bonds with the consolidated material, obtaining a homogeneous coating with a few small pores, despite the large difference in particle size. During the process, the particles of the coating material are plastically deformed and bond with the substrate and with each other as a consequence of mechanical anchoring of particles and adiabatic shear instability. Coating after cold spraying Fig. 3a. showed a very dense microstructure with negligible porosity, which appears in the form of small interlamellar voids (white arrows) and bigger pores between incompletely deformed particles (black arrows). The magnified view of the coating revealed very good cohesion between significantly deformed powder grains (Fig. 4b). The tested Ni20Cr coating is characterized by good adhesion to the substrate (Fig. 3b), there were no visible voids at the interface of the coating with the substrate.

The microstructure of the coating after laser melting is shown in Fig. 4. Laser processing essentially reduced pores, providing a more homogeneous and dense microstructure. On the cross-section, the laser processing zone can be clearly distinguished, Fig. 4a. The laser surface melting is 70 µm±5 coating depth, which is 1/3 of the coating thickness in Fig. 4a. In the laser surface melted coating zone, the columnar structure was formed (Fig. 4b(2)), on the surface of which a thin layer of fine elongated grains is visible, arranged parallel to the substrate (Fig. 4b(1)). There are no visible cracks in the cross-section of the coating. Properly performed laser surface melting is associated with a high energy density supplied to the intended place, which minimizes the amount of this energy and the possibility to cracks which are reported in some cases [26]. There are two kinds of porosity in the coating area (Fig. 4b): initial porosity formed during cold spraying, irregularly shaped, placed along grains' boundaries, and second one- gas bubbles -in laser melted part, coming from trapped argon. The melting process causes the disappearance of the boundaries between the deformed powder grains, the existing pores disappear and the gas from them is released on the surface, and the porosity of the laser melted layer is negligible. The porosity of the laser melted coating was reduced to 0.44±27 %vol. compared to the porosity of the cold sprayed coating of 2.7±83 %vol. Such a significant decrease in porosity occurs in any case of laser melting of a thermally sprayed coating [26-28]. Etched a cross-section of laser melted coating (Fig. 4b) clearly

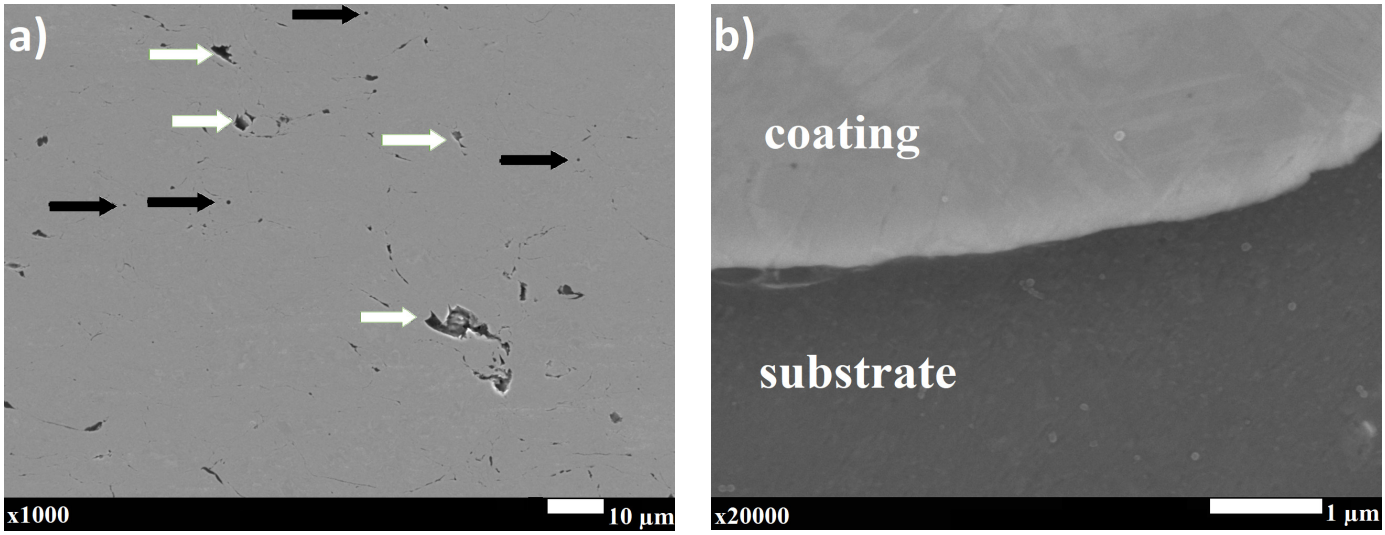

Fig. 3. Microstructure of the cold sprayed Ni20Cr coating a) 1000×, b) 20000×

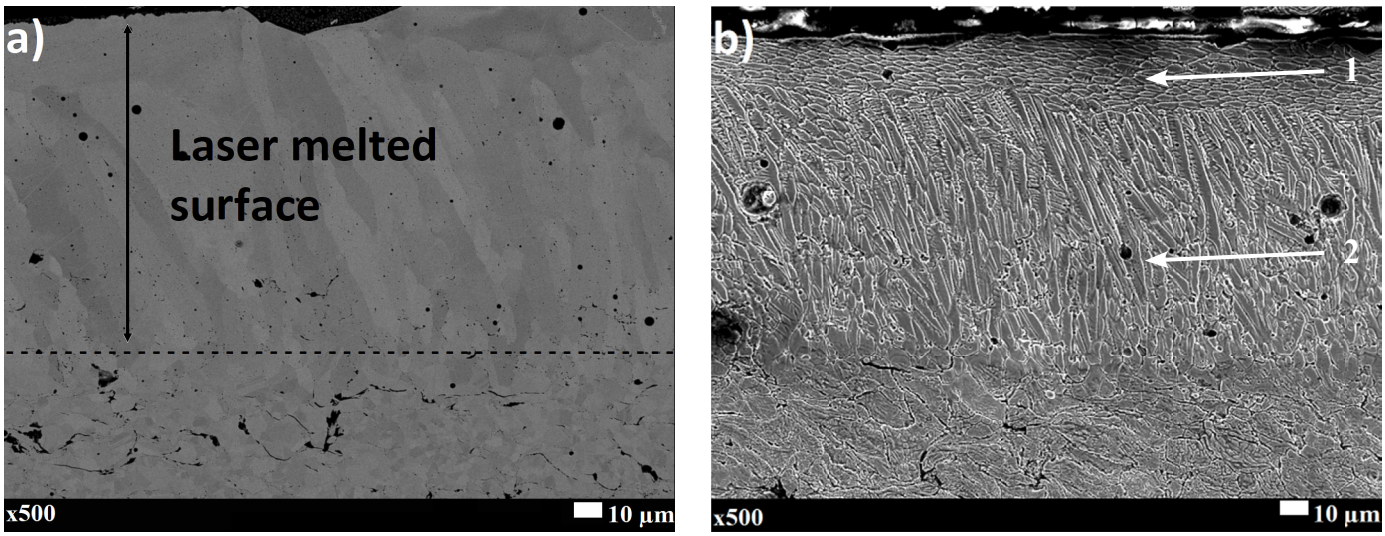

Fig. 4. Microstructure of the cold sprayed Ni20Cr coating after laser melting a) general view, b) general view, samples after etching

shows the differences in the microstructure of the cold spray coating before and after laser melting. The lamellar structure of cold sprayed coating consisting of significantly deformed Ni20Cr grains melted with a laser beam (bottom of Fig. 4b) changed into the columnar structure. The columnar grains visible on etched cross-section indicate that grew in the direction perpendicular to the movement of the laser. The same columnar microstructure was obtained by 2014 Song at al. [29] using the same powder in the Laser Sintering Melting (LSM) process to make the tensile specimens. There are several spherical small holes visible in the cross-section of the laser melted coating. The small holes formed in the coating surface during laser melting are gas bubbles that can be attributed to the release of trapped gas during melting. The laser melting process was very short and the thickness of the molten material was large compared to the dimensions of the gas bubbles, as a consequence rapid solidification of melted coating prevented escaping the gas bubbles from melting material and leaving small holes in the melted coating. The gas bubbles which have not been reached the surface of the coating have formed small round pores inside the melted layer. Such pores are present in laser melted thermal spray coatings [30-32].

Fig. 5 and Fig. 6 show the distribution maps of chemical elements (Ni, Cr, O) before and after laser surface melting, made with the energy dispersion spectroscopy (EDS). In the presented distribution of elements, it can be seen that the degree of homogenization of Ni and Cr elements in these coatings is very high. These two elements are distributed evenly in the coatings, no concentration of the elements in one place was found, so it can be concluded that there is no significant difference in the chemical composition of both coatings. The presence of oxygen in the cross-sections of both coatings is visible exactly only in the place where pores are present (Fig. 5d and 6d). These figures additionally confirm a significant decrease in porosity in laser melted coating calculated from digital image analysis. Lack of oxygen in other places on the cross-section of laser melted coating means that no oxides were formed in it, which could be the result of laser melting of the cold sprayed coating.

XRD analysis showed that the results of the cold gas sprayed coatings are consistent with the original results of the Ni20Cr powder in Fig. 2. Thus, the mechanism of deposition of the cold gas spray took place in a solid-state and, the maximum gas temperature did not exceed 800°C and decreases very quickly during the process, so there were no changes in the crystallographic phase in the structure, which is a significant advantage of this process. There is no change in phase composition during cold spraying process, which is seen with traditional thermal spray methods. No phase change is related to low temperature occurring when spraying with cold gas because this process takes place at a temperature lower than the melting point of the sprayed coating material [25]. Laser melting carried out in the next stage of research and the associated laser surface melting of the coating causes the formation of oxides on the surface of the coating. The oxides; NiO, NiO_2, CrO and Cr_2O_3 are the result of the oxidation process during laser melting as presented in Fig. 2. Compared with the diffraction pattern of the cold gas sprayed coating, small peaks due to the presence of oxides of the main coating components, i.e. nickel and chromium, are visible. Measurements of hardness showed an increase in microhardness and Young's modulus (E) compared to coatings sprayed with cold gas without laser melting (Table 3).

TABLE 3

Mechanical properties of Ni20Cr cold sprayed coatings

Parameter	Cold sprayed coating	After laser surface melting
HV0.3	388 ± 37	454 ± 32
E, GPa	54.2 ± 4	67.4 ± 5

Porosity and voids in the microstructure of the obtained coating when spraying with cold gas are an important issue related to the mechanical properties of the coatings. The hardness value for the coating sprayed with cold gas was 388 HV0.3±37 and was 84% higher than those corresponding to the bulk

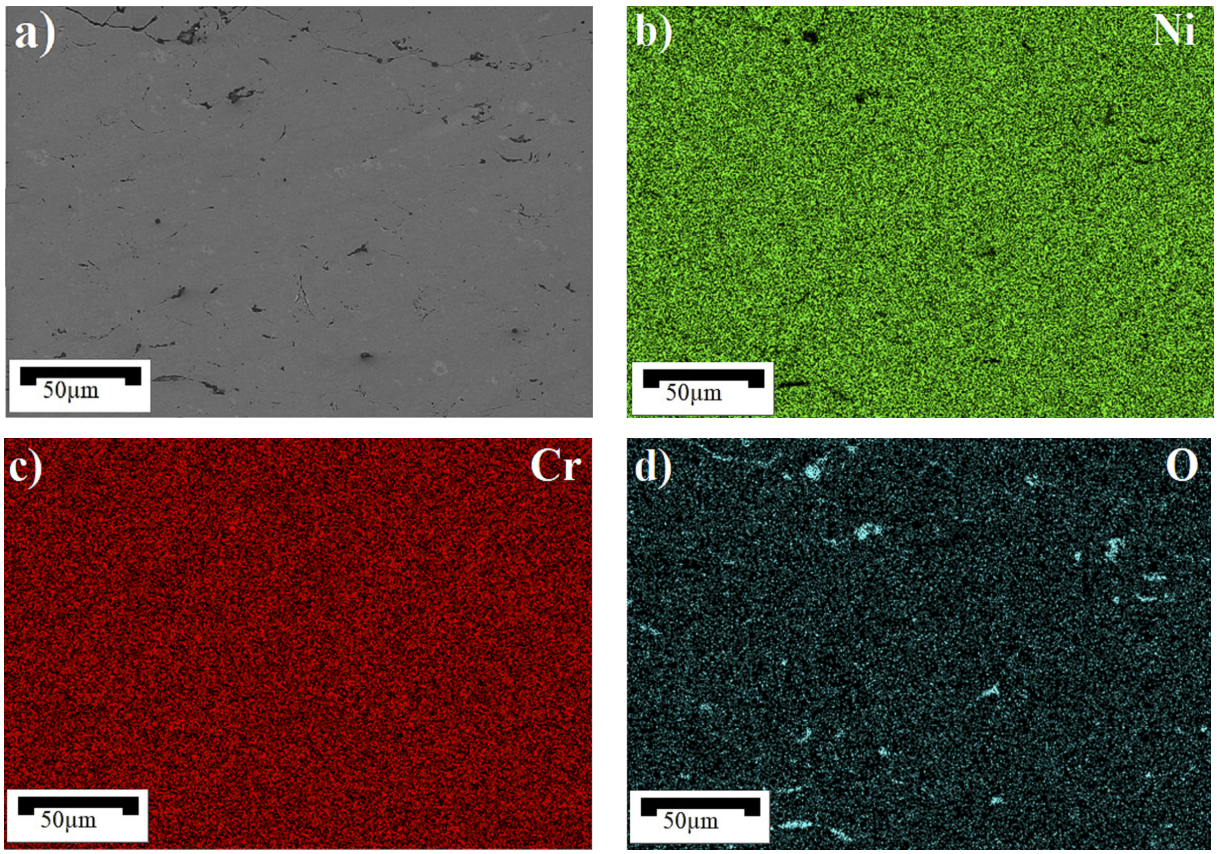

Fig. 5. Map of the distribution of elements a) SEM image of the microstructure of Ni20Cr coating, b), c) and d) maps of Ni, Cr and O distribution, respectively

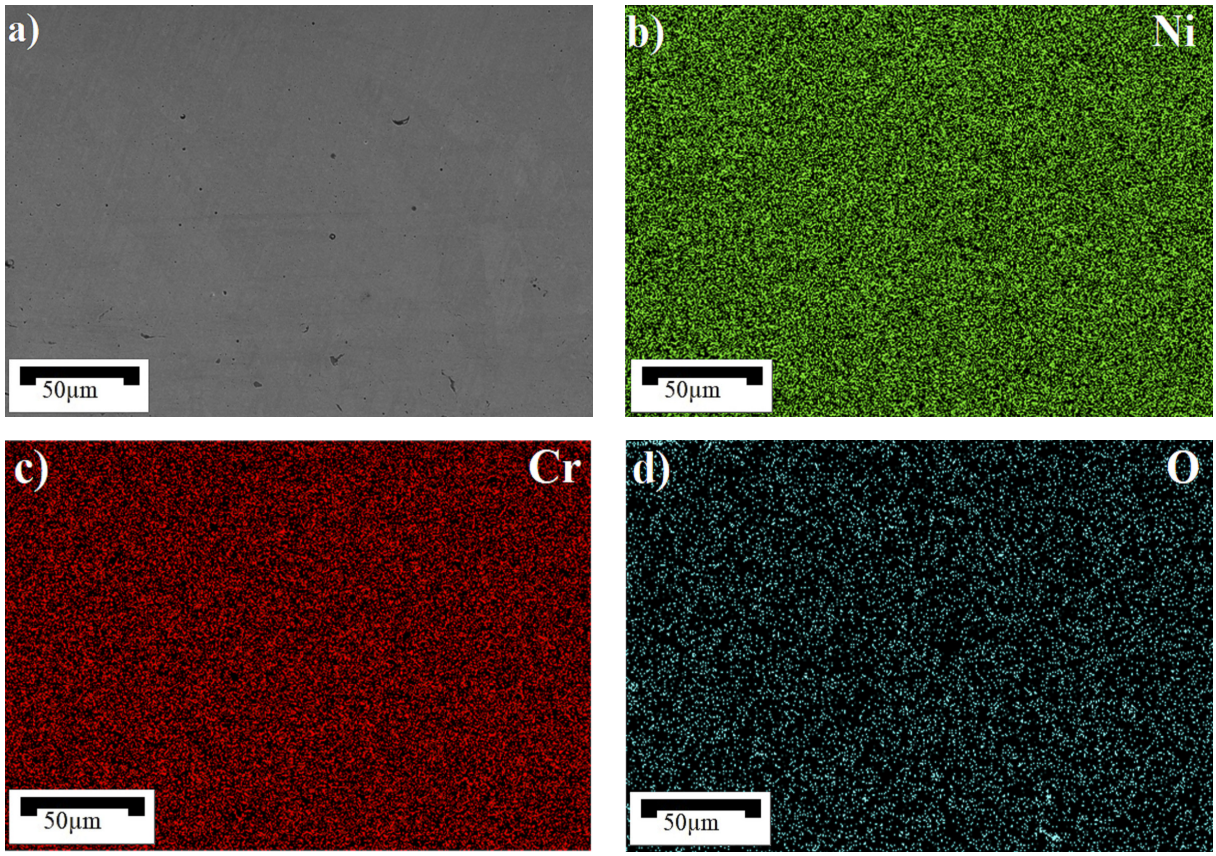

Fig. 6. Map of the distribution of elements a) SEM image of the microstructure of Ni20Cr coating after laser melting, b), c) and d) maps of Ni, Cr and O distribution, respectively

alloy – 211 HV. Such a significant increase in hardness is the effect of the work hardening process resulting from the particles hitting the formed coating and their plastic deformation during the cold spray process. Similar effect have also been reported by other authors [33-35]. Laser surface melting significantly affected the elimination of porosity, thus obtaining a uniform and compact microstructure. After laser surface melting the microhardness of the coating increased to 454 HV0.3±32 and was 17% higher than the hardness of the cold sprayed coating. This hardening effect of the laser melting surface is caused by a surface melting and rapid cooling process. Surface melting with the high power density of the laser beam and simultaneous fast cooling makes immediate solidification of the melted coating. At the same time, the very high power density of the laser beam creates a very high temperature gradient in the melted material. Such conditions result in the formation of a columnar structure, the thickness of which is approximately equal to the depth at which the coating is melted. Such columnar microstructure is more uniform than the microstructure of cold sprayed coating which makes it harder. Moreover, the porosity of the obtained Ni20Cr coating in the laser surface melting zone is much lower (0,44%±0,27) than that of the cold sprayed coating (2.7%±0,83). Significant reduction in porosity and, consequently, densification of the laser melting microstructure is the additional factor increasing the hardness of the coating. The carried out tests showed that the elastic modulus was higher for the coating with a laser melted surface. This can be attributed to the more uniform microstructure and lower porosity after laser modification. The value for the cold gas spray coating was 54.2 GPa and for the laser surface melting coating was 67.4 GPa. The reduction of porosity increased Young's modulus of the Ni20Cr coating and the increase amounted to approx. 24%. P. Poza et al. [28], while examining the mechanical properties of Inconel 625 cold-sprayed coatings after laser melting, also observed an increase in the elasticity modulus of the coating after laser surface melting.

The laser surface melting also caused significant changes in the surface morphology of the coatings. The surface of the coatings was optically scanned and the measured data was used to characterize the height parameters according to ISO 25178 [36]. The structure of the measured surfaces was described using the Abbott-Firestone curve. Figures 7 and 8 show surface

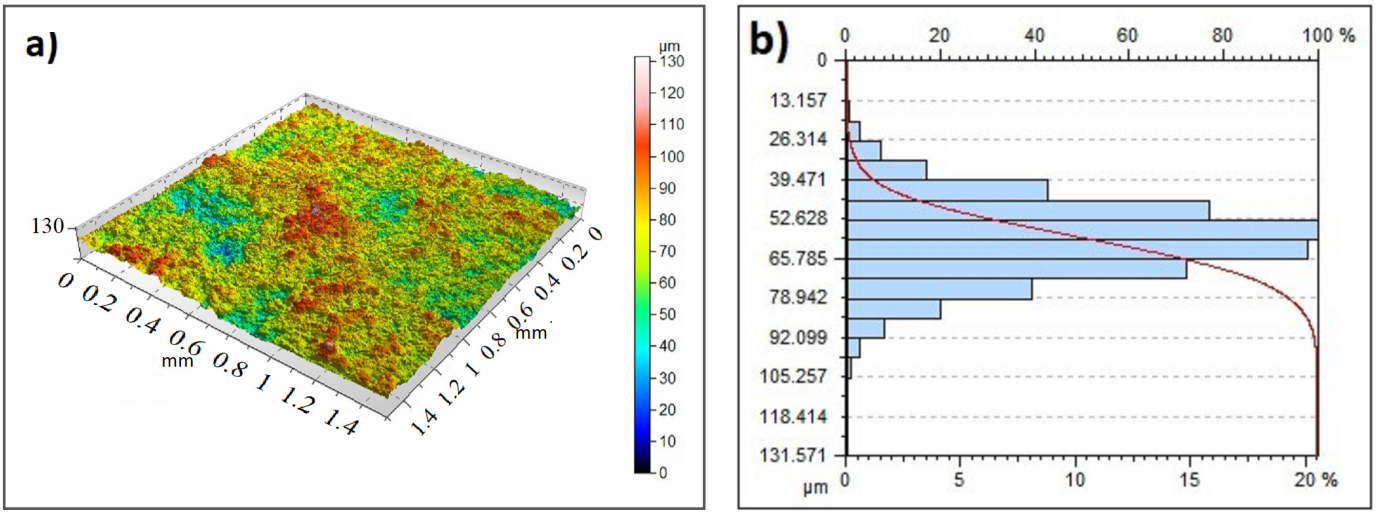

Fig. 7. Cold sprayed Ni20Cr coating: a) surface morphology, b) depth histogram and bearing curve

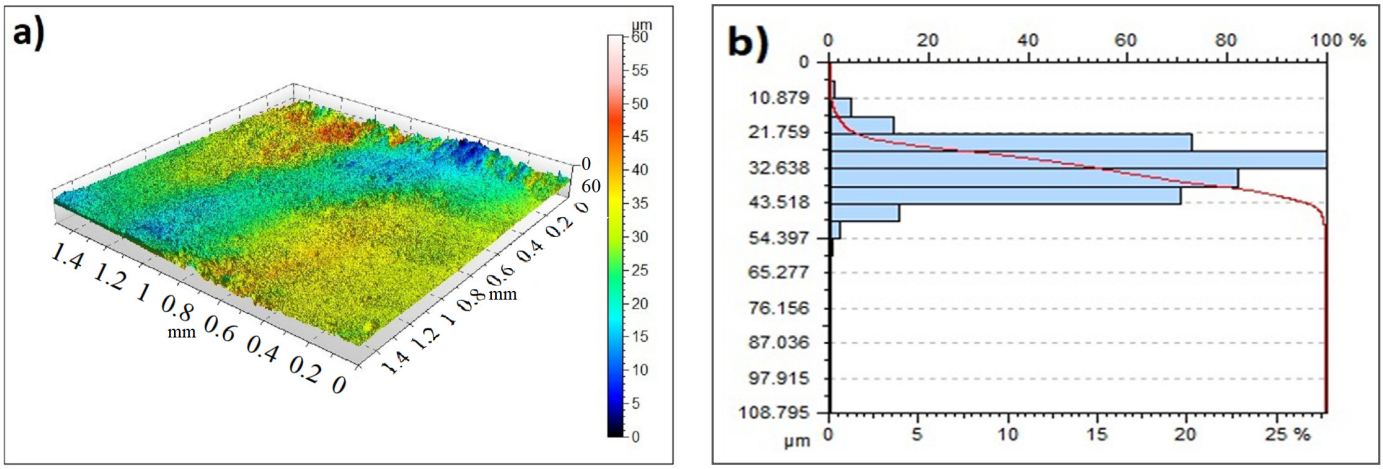

Fig. 8. Laser melted cold sprayed Ni20Cr coating: a) surface morphology, b) depth histogram and bearing curve

topographies, depth histograms and bearing support curves for Ni20Cr cold spray coatings before and after laser surface melting [37,38]. The slope of the bearing surface curve after laser processing is much smaller, which results in a smoother surface. The obtained results show that the coatings are characterized by high toughness. The arithmetic mean of the height (Sa) describing the height changes for the cold sprayed Ni20Cr coatings was 10.04 µm, and for the coatings after laser surface melting it was 5.81 µm, which means it decreased almost twice (Table 4). The average height of the square root (Sq) of the coating after laser surface melting is 45% lower than that of the cold-sprayed only coating, which indicates a stronger adhesive and mechanical effect. The cold sprayed Ni20Cr coatings showed surface height asymmetry (Ssk = –0.07) with a negative skew. This proves the concentration of structures with deeper and sharper valleys. The asymmetry of the height of the coating surface after laser surface melting (Ssk = 0.07) was positive, which proves a smoother coating surface. The Sku kurtosis value for the tested coatings results from the absence of extreme peaks or valley features and is 3.23 for the cold spray coating and 2.92 for the laser surface melted coating. Other topography parameters such as maximum peak height (Sp), maximum surface height (Sz), maximum surface indentation (Sv) are lower after laser surface melting, which confirms the flatness of the sample surface. It can be concluded that the surface morphology of cold sprayed coatings strongly depends on laser surface melting.

TABLE 4

Surface topography parameters according to ISO 25178

Parameter	Cold sprayed coating	After laser surface melting
Sa [µm]	10.04	5.81
Sq [µm]	12.73	7.01
Ssk	–0.07	0.07
Sku	3.23	2.92
Sp [µm]	59.20	32.28
Sv [µm]	72.37	76.52
Sz [µm]	131.570	108.795

4. Conclusion

The paper presents the influence of laser processing on the microstructure and mechanical properties of Ni20Cr cold sprayed coatings onto an aluminum alloy 7075 substrate. The high kinetic energy of the powder particles during the process caused their significant deformation, which leads to their strong cohesion. Coatings after the cold spray process have the same phase composition as the applied powder. The Ni20Cr coatings sprayed with cold gas show negligible porosity. Only small pores are visible under high magnification. Laser melting changed phase composition of produced coating as the effect of Cr and Ni oxidation, increase in the hardness and Young's modulus of the deposit and decrease in surface roughness.

REFERENCES

[1] L. Pawlowski, The science and engineering of thermal spray coatings, J. Willey & Sons Ltd, Chichester, II ed. (2008).

[2] D. Tejero-Martin, M. Rezvani Rad, A. McDonald, T. Hussain, J. Therm. Spray Technol. **28** (4), 598-644 (2019).

[3] G. Di Girolamo, E. Serra, Thermally Sprayed Nanostructured Coatings for Anti-wear and TBC Applications: State-of-the-art and Future Perspectives, Anti-Abrasive Nanocoatings, Ed., Woodhead Publishing Limited, 513-541 (2015). DOI: https://doi.org/10.1016/B978-0-85709-211-3.00020-0

[4] A. Góral, L. Lityńska-Dobrzyńska, W. Żórawski, K. Berent, J. Wojewoda-Budka, Arch. Metall. Mater. **58** (2), 335-339 (2013).

[5] C.M. Kay, J. Karthikeyan, High Pressure Cold Spray, ASM International 2016.

[6] H. Assadi, H. Kreye, F. Gartner, T. Klassen, Acta Materialia **116**, 382-407 (2016).

[7] M.R. Rokni, S.R. Nutt, C.A. Widener, G.A. Crawford, V.K. Champagne, Springer. **5**, 143-192 (2018).

[8] A. Góral, W. Żórawski, P. Czaja, L. Lityńska-Dobrzyńska, M. Makrenek, S. Kowalski, J. Mater. Res. **110**, 49-59 (2019), DOI: 10.3139/146.111698

[9] Q. Wang, N. Birbilis, X. Zahang, Metall. Mater. Trans. A Phys. Metall. Mater. Sci. **43**, 1395-1399 (2012),

[10] C.W. Ziemian, M.M. Sharma, B.D. Bouffard, T. Nissly, T. Eden, Mater. Des. **54**, 212-221(2014)

[11] L. Ajdelsztajn, B. Jodoin, J.M. Schoenung, Surf. Coat. Tech. **201**, 1166-1172 (2006).

[12] M. Scendo, W. Żórawski, A. Góral, Metals **9**, 890-910 (2019). DOI:103390/met9080890

[13] E. Qin, B. Wang, W. Li, Ma, H. Lu, S. Wu, J. Therm. Spray Technol. **28**, 1072-1080 (2019).

[14] D. Kong, B. Zhao, J. Alloys Compd. **705**, 700-707 (2017).

[15] T. Otmianowski, B. Antoszewski, W. Żórawski, Proceesing of 15th International Thermal Spray Conference, 25-29 May, Nice, France, 1333-1336 (1998).

[16] B. Antoszewski, P. Sęk, Proc. SPIE **8703**, 8703-8743 (2012). DOI: https://doi.org/10.1117/12.2015240

[17] P. Sęk, Open Eng. **10**, 454-461 (2020).

[18] M. Tlotleng, M. Shukla, E. Akinlabi, S. Pityana, Surface Engineering Techniques and Application: Research Advancements 177- 221 (2014). DOI: https://doi.org/10.4018/978-1-4666-5141-8.ch006

[19] D.K. Christoulis, M. Jeandin, E. Irissou, J.G. Legoux, W. Knapp, Laser-Assisted Cold Spray (LACS) InTech. 59-96 (2012). DOI: https://doi.org/10.5772/36104

[20] S.B. Mishra, K. Chandra, S. Prakash, J. Tribol. **128**, 469-475 (2006) DOI:10.1115/1.2197843

[21] A. Mangla, V. Chawla, G. Singh, Int. J. Eng. Sci. Res. Technol. **6**, 674-686 (2017).

[22] N. Abu-Warda, A.J. López, M.D. López, M.V. Utrilla, Surf. Coat. Tech. **381**, 125133 (2020).

[23] EN ISO 6507-1: 2018.

[24] https://www.scribd.com/document/423195204/DSMTS-0109-2-Ni20Cr-Powders

[25] A. Góral, W. Żórawski, M. Makrenek, Surf. Coat.Tech. **361**, 9-18 (2019).
[26] S.H. Zhang, T.Y. Cho, J.H. Yoon, W. Fang, K.O. Song, M.X. Li, Y. K. Joo, C.G. Lee, Charact. **59**, 1412-1418 (2008).
[27] N. Serres, F. Hlawka, S. Costil, C. Langlade, F. Machi, J. Therm. Spray Technol. **20**, 336-343 (2011).
[28] P. Poza, C.J. Munez, M.A. Garrido-Maneiro, S. Vezzu, S. Rech, A. Trentin, Surf. Coat. Tech. **243**, 51-57 (2014).
[29] B. Song, S. Dong, P. Coddet, H. Liao, C. Codde, Mater. Dec. **53**, 1-7 (2014).
[30] P. Serra, J.M. Miguel, J.L. Morenza, J.M. Guilemany, J. Mater. Res. **16**, 3416-3422 (2001).
[31] A. Góral, W. Żórawski, L. Litynska-Dobrzyńska, M. Makrenek, M. Goły, A. Trelka, Surf. Coat.Tech. **405**, 126701 (2021).
[32] J. Mateos, J.M. Cuetos, E. Ferna´ndez, R. Vijande, Wear **239**, 274 (2000).
[33] C. Navas, R. Vijande, J.M. Cuetos, M.R. Fernández, J. de Damborenea, Surf. Coat.Tech. **235**, 776-785 (2006).
[34] Y. Zhang, X.F. Gao, X. Liang, K. Chong, D. Wu, Y. Zou, Surf Coat Tech. **398**, 126099 (2020).
[35] A. Sova, S. Grigoriev, A. Okunkova, I. Smurov, Surf. Coat.Tech. **235**, 283-289 (2013).
[36] EN ISO 25178 (2012).
[37] S. Adamczak, D. Janecki, K. Stępień, Measurement **44** (1), 164-173 (2011).
[38] D. Janecki, K. Stepień, S. Adamczak, Measurement **43**, 659-663 (2010).